

UC Santa Barbara

UC Santa Barbara Previously Published Works

Title

Changes in above- versus belowground biomass distribution in permafrost regions in response to climate warming

Permalink

<https://escholarship.org/uc/item/2472d5wh>

Journal

Proceedings of the National Academy of Sciences of the United States of America, 121(25)

ISSN

0027-8424

Authors

Yun, Hanbo
Ciais, Philippe
Zhu, Qing
[et al.](#)

Publication Date

2024-06-18













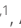


DOI

10.1073/pnas.2314036121

Peer reviewed



Changes in above- versus belowground biomass distribution in permafrost regions in response to climate warming

Hanbo Yun^{a,b,c,d} , Philippe Ciais^e , Qing Zhu^f , Deliang Chen^g , Constantin M. Zohner^{h,1} , Jing Tang^h , Yang Qu^k , Hao Zhou^l , Joshua Schimel^l , Peng Zhu^{m,n} , Ming Shao^o , Jens Hesselbjerg Christensen^p , Qingbai Wu^{a,b,1} , Anping Chen^q , and Bo Elberling^{c,1} 

Edited by Nils Stenseth, Universitetet i Oslo, Oslo, Norway; received August 21, 2023; accepted May 4, 2024

Permafrost regions contain approximately half of the carbon stored in land ecosystems and have warmed at least twice as much as any other biome. This warming has influenced vegetation activity, leading to changes in plant composition, physiology, and biomass storage in aboveground and belowground components, ultimately impacting ecosystem carbon balance. Yet, little is known about the causes and magnitude of long-term changes in the above- to belowground biomass ratio of plants (η). Here, we analyzed η values using 3,013 plots and 26,337 species-specific measurements across eight sites on the Tibetan Plateau from 1995 to 2021. Our analysis revealed distinct temporal trends in η for three vegetation types: a 17% increase in alpine wetlands, and a decrease of 26% and 48% in alpine meadows and alpine steppes, respectively. These trends were primarily driven by temperature-induced growth preferences rather than shifts in plant species composition. Our findings indicate that in wetter ecosystems, climate warming promotes aboveground plant growth, while in drier ecosystems, such as alpine meadows and alpine steppes, plants allocate more biomass belowground. Furthermore, we observed a threefold strengthening of the warming effect on η over the past 27 y. Soil moisture was found to modulate the sensitivity of η to soil temperature in alpine meadows and alpine steppes, but not in alpine wetlands. Our results contribute to a better understanding of the processes driving the response of biomass distribution to climate warming, which is crucial for predicting the future carbon trajectory of permafrost ecosystems and climate feedback.

vegetation adaptations | permafrost | climate warming | biomass allocation | carbon trajectory

Rapid warming in alpine permafrost regions is driving changes in plant growth (1), abundance (2), and species composition (3, 4), which determines plant aboveground versus belowground biomass distribution and exerts feedback on the carbon cycle (5). Changes in plant biomass allocation and turnover can alter the rate of soil organic carbon (SOC) accumulation and mineralization (6, 7) and facilitate the mineralization of old soil organic matter (SOM) by enhancing the content of labile carbon substrates and available nitrogen. These processes can stimulate microbial decomposition (8, 9) and ultimately increase soil CO₂ emissions (8, 10).

Multiple lines of evidence suggest that climate change will cause shifts in above- and belowground plant biomass in permafrost ecosystems (11, 12). For instance, warmer and moister summers led to greater biomass allocation toward leaves and stems to absorb more light and CO₂ (13–15). Conversely, some studies have shown that root length has increased by 30 to 140% allowing plants to acquire more nitrogen from thawed permafrost (16–18), while decadal-scale aboveground biomass has remained steady (18, 19).

Although plants have been shown to adjust their above- and belowground biomass growth differentially in response to climate change (20, 21), there is a limited understanding of the changes in the above- to belowground biomass ratio (hereafter referred to as η), which provides a holistic metric for assessing plant resource acquisition. Competing hypotheses exist regarding how η responds to climate warming. These include species shifts resulting from resource competition, and plant allocation adjustments within the same species to optimize resource acquisition. In permafrost-affected ecosystems, η is expected to be sensitive to soil warming and permafrost thawing (14), as increased mineralization within the active layer is linked to nitrogen release from thawing permafrost (18). Other mechanisms can also alter η , potentially amplifying or counteracting changes predicted by soil temperature alone. For example, a decline in the soil water table can increase the abundance of long-root species and reshape plant community composition, ultimately leading to a decrease in η as observed in Arctic grasslands (1, 22). Conversely, extreme drought can stimulate plants to allocate more biomass into propagules without affecting root growth, thereby enhancing η in tundra ecosystems (23, 24). However, given

Significance

Quantification of changes in the above- to belowground biomass ratio of plants (η) is needed to improve and constrain estimates of carbon budgets. Here, we quantify temporal and spatial trends (27 y) of η and its environmental controls in the Tibetan Plateau. We show that η has increased by 17% in alpine wetlands but decreased by 26 and 48% in alpine meadows and alpine steppes. These shifts were mainly driven by temperature-induced changes in growth. A threefold strengthening of the warming effect on η was observed over the years. We further show that current ecosystem models do not capture the observed variation in η . Our results are therefore crucial for predictions of the future carbon trajectory of alpine ecosystems.

Author contributions: H.Y., P.C., A.C., and B.E. designed research; D.C., C.M.Z., and Q.W. performed research; Y.Q., H.Z., and J.H.C. contributed new reagents/analytic tools; Q.Z., C.M.Z., J.T., P.Z., M.S., Q.W., and B.E. analyzed data; and H.Y., P.C., C.M.Z., J.S., J.H.C., and B.E. wrote the paper.

The authors declare no competing interest.

This article is a PNAS Direct Submission.

Copyright © 2024 the Author(s). Published by PNAS. This article is distributed under [Creative Commons Attribution-NonCommercial-NoDerivatives License 4.0 \(CC BY-NC-ND\)](https://creativecommons.org/licenses/by-nc-nd/4.0/).

¹To whom correspondence may be addressed. Email: constantin.zohner@gmail.com, qbwu@lzb.ac.cn, or be@ign.ku.dk.

This article contains supporting information online at <https://www.pnas.org/lookup/suppl/doi:10.1073/pnas.2314036121/-/DCSupplemental>.

Published June 10, 2024.

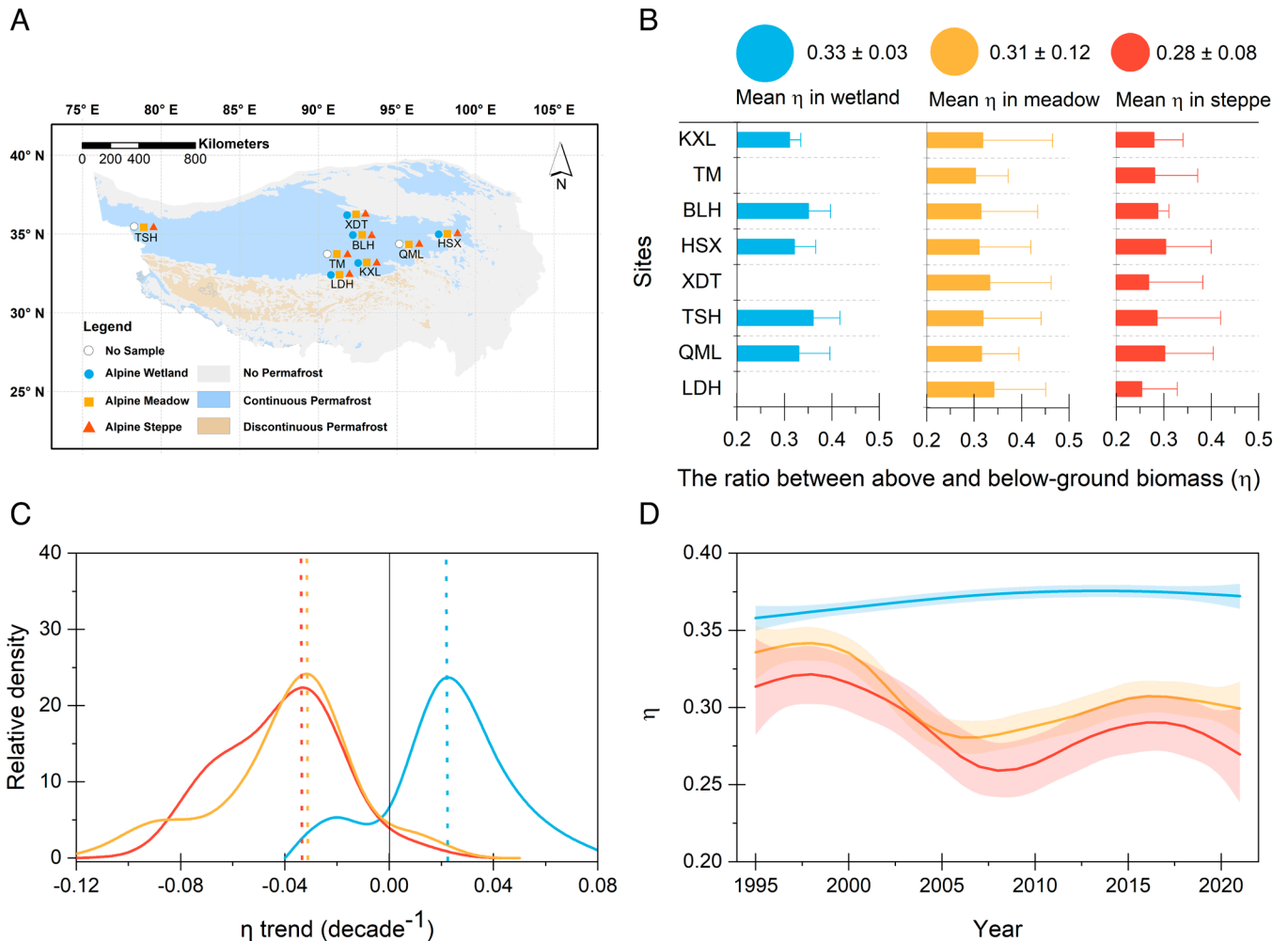


Fig. 1. Locations of study sites, the mean values of the ratio between aboveground and belowground biomass (η ; mean \pm SD) and its temporal trend with vegetation types of alpine wetland (blue), alpine meadow (orange), and alpine steppe (red) from 1995 to 2021. (A) Spatial distribution of sites. (B) Estimated plot-level η in three major alpine ecosystems on the Tibetan Plateau: i) alpine wetlands, including 680 plots from five sites calculated from the six to eight dominant plant species; ii) alpine meadows, including 1,214 plots from eight sites calculated from the 8 to 12 dominant plant species; and iii) alpine steppes, including 1,119 plots from eight sites calculated from the 8 to 12 dominant plant species. (C) Density of decadal-scale trend magnitudes of estimated plot-level η in alpine wetland (blue line; $n = 108$), alpine meadow (orange line; $n = 192$), and alpine steppe (red line; $n = 285$) (decade⁻¹) during 1995 to 2021. The x axis range for each vegetation type covers two SD from the median, or approximately 95% of the data. The vertical dashed lines indicate median trends, and the zero trend is highlighted by a black vertical line. (D) Smoothed curves of generalized additive mixed models (GAMMs) for the alpine wetlands (blue line; $n = 680$), alpine meadows (orange line; $n = 1,214$), and alpine steppes (red line; $n = 1,119$), showing deviation from the mean model predictions for selected response variables with year as the predictor variable. The blue, orange, and red shading represent one SE from the predicted line for estimated plot-level η over time across the Tibetan Plateau. Plots that were less than 15 y old were excluded from the GAMMs analysis.

the complex, interactive nature of the processes regulating η , its overall trajectories remain poorly understood (25, 26).

While process-based biogeochemistry models are valuable tools for estimating vegetation biomass in permafrost ecosystems, they currently lack the ability to adequately account for changes in η that occur in response to climate change (27, 28). This limitation can result in inaccurate predictions of ecosystem carbon cycling and storage and nutrient and water acquisition (28). Improving our understanding of how plant biomass distribution responds to changing environmental conditions and incorporating this knowledge into biogeochemical models will be crucial for accurately projecting the impacts of climate change on permafrost ecosystems (8, 29).

To improve our understanding of how η changes in response to environmental changes in permafrost ecosystems, our study focused on long-term changes (1995 to 2021) of η within 3,013 plots at eight stations on the Tibetan Plateau, encompassing three core alpine vegetation types. Our analysis addressed two fundamental questions: 1) How did η change over recent decades in

response to rapid climate warming in permafrost ecosystems? 2) What are the dominant drivers of the variations in η ?

Results

Variation in Biomass Distribution Over Time. Our measurements showed that the mean of the ratio between above- and belowground biomass (η) in alpine wetlands was 0.33 ± 0.03 and increased by 0.06 ± 0.05 from 1995 to 2021. Conversely, in alpine meadows and steppe, mean plot-level η was 0.31 ± 0.2 and 0.28 ± 0.08 , respectively, and decreased by -0.08 ± 0.05 and -0.13 ± 0.06 from 1995 to 2021 (Fig. 1 B and C). These changes in η represent a relative increase of 17% for the alpine wetlands and decreases of 26% and 48% in alpine meadows and alpine steppes, respectively. To assess the linearity of temporal variation in η , we used effective degrees of freedom (edf). The edf for alpine wetlands was 1.6, indicating a nearly linear relationship between predictor variables (year) and η . However, in alpine meadows and steppes, the edf values were 8.7 and 9.1, respectively, indicating more complex

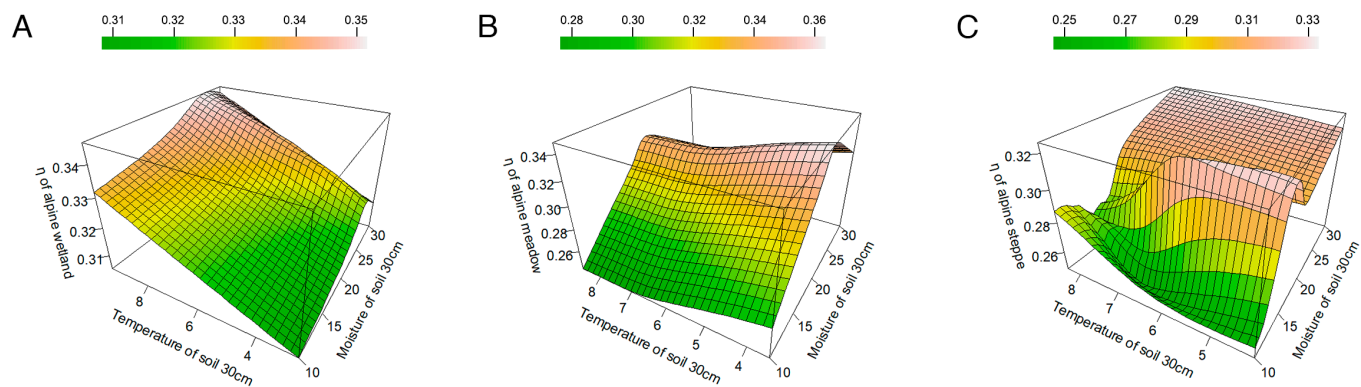


Fig. 2. Interactions between estimated mean plot-level η values and soil temperature ($^{\circ}\text{C}$) and moisture (%) during the growing season for the alpine wetlands (A), alpine meadows (B), and alpine steppes (C). Trends are based on GAMMs. We only included sites at which all three ecosystem types are present, i.e., the analysis includes the sites KXL, BLH, HSX, TSH, and QML, while omitting OML, TM, and TSH to ensure a consistent comparison framework.

patterns over time (Fig. 1D and *SI Appendix*, Figs. S1–S3). Although plot-level η generally increased over time in wetlands and decreased in alpine meadows and steppe, the temporal trends in η were species-specific within each vegetation type (*SI Appendix*, Table S1). For example, at the alpine steppe site HSX, η decreased significantly ($P < 0.01$) in more than half of the plant species (nine species recorded in each plot), while three other species showed no significant changes ($P > 0.05$). We also observed high variation in the temporal trajectory of η within species. For instance, *Carex moorcroftii* (hereafter referred to as *Carex*) showed decreases at three sites (BLH, HSX, and QML; $P < 0.01$), while no significant changes were found at two sites (TM and XDT; $P > 0.05$), and significant increases occurred at two sites (KXL and TSH; $P < 0.01$) (*SI Appendix*, Table S1).

Driver of Spatial and Temporal Variation in η . GAMMs revealed a positive correlation between spatial variations in estimated plot-level η and soil temperature in alpine wetlands. In contrast, in alpine meadow and steppe vegetation, we observed lower η with higher soil temperature (Fig. 2). However, there was substantial variability between sites and species in alpine meadows and steppe, with some sites or species exhibiting increases in both soil temperature and η (Fig. 2 and *SI Appendix*, Fig. S4). For instance, at alpine meadows and steppe sites with high soil moisture ($>25\%$), η increased with increasing soil temperature. Consistent with the GAMM results, our causality analysis (convergent cross-mapping) showed that soil temperature during the growing season was the major climatic driver of η variation in all vegetation types (*SI Appendix*, Fig. S5). Specifically, alpine wetlands showed opposite responses of η to higher soil temperature compared to alpine meadows and steppe vegetation.

Between 1995 and 2021, estimated plot-level η increased in alpine wetlands, where 56.9% of the samples of all six plant species showed a positive trend in aboveground biomass ($>3.5 \text{ g decade}^{-1} \text{ species}^{-1}$) while almost no change in belowground biomass was found for each time series ($< 1.0 \text{ g decade}^{-1} \text{ species}^{-1}$) (Fig. 3A and *SI Appendix*, Fig. S6). This increase in aboveground biomass was best explained by a soil warming of $0.11 \text{ }^{\circ}\text{C decade}^{-1}$ (standardized coefficient (Beta) = 0.51 and $P < 0.01$) (*SI Appendix*, Table S2). The changes could not be explained by soil moisture, which was relatively stable over time ($P > 0.05$) (*SI Appendix*, Fig. S7). The soil warming trend was best explained by increasing air temperature during the growing season and a reduced frequency of precipitation (adj. $R^2 = 0.67$ and $P < 0.01$) (*SI Appendix*, Table S3). Among the six studied species, those with higher initial aboveground biomass showed stronger increases in η ($R^2 = 0.23$),

but higher belowground biomass was not related to the estimated plot-level η trend ($R^2 = 0.09$) (*SI Appendix*, Fig. S8).

The estimated plot-level η in alpine meadow and steppe exhibited multidecadal oscillations from 1995 to 2020 (Fig. 1D), with above- and belowground biomass showing divergent temporal trends (Fig. 3D and C). Although more than half of the samples in both vegetation types showed a positive trend in both above- and belowground biomass, a substantial proportion (21.2%) of samples showed almost no change in aboveground biomass ($<1.0 \text{ g decade}^{-1}$) and a decreasing trend in belowground biomass ($>-3.5 \text{ g decade}^{-1}$) in the alpine meadow. In the alpine steppe, 22.4% of samples showed a negative trend ($-2.7 \text{ g decade}^{-1}$) in aboveground biomass but a positive trend in belowground biomass ($4.6 \text{ g decade}^{-1}$) (Fig. 3 and *SI Appendix*, Fig. S6). In alpine meadow and alpine steppe, 8 and 12 studied plant species, respectively, plant species with higher above- and belowground biomass showed a stronger decreasing trend in η ($R^2 = 0.17$ to 0.24) (*SI Appendix*, Fig. S8). For instance, in the alpine steppe at site HSX, the plant species *Heteropappus bowerii*, which has a higher above- and belowground biomass than in all the other species, exhibited a more pronounced decreasing trend in η compared to the other eight plant species studied (*SI Appendix*, Fig. S9).

The temporal variation in aboveground and belowground biomass in alpine meadow and alpine steppe were primarily correlated with changes in soil temperature and moisture. In alpine meadow, the increase in soil temperature at a rate of $0.3 \text{ }^{\circ}\text{C decade}^{-1}$ (*SI Appendix*, Fig. S7) was correlated with a decreasing trend in biomass (Beta = -0.40 , $P < 0.01$) (*SI Appendix*, Tables S2 and S4). Similarly, in alpine steppe, the soil temperature increases of $0.5 \text{ }^{\circ}\text{C decade}^{-1}$ (*SI Appendix*, Fig. S7) led to a decrease in biomass (Beta = -0.49 , $P < 0.01$) (*SI Appendix*, Tables S2 and S4). The decreasing trend in soil moisture of 3% and 5% per decade in alpine meadow and alpine steppe, respectively (*SI Appendix*, Fig. S7), also had a significant impact on biomass (Beta = 0.18, $P = 0.052$ in alpine meadow and Beta = 0.26, $P < 0.05$ in alpine steppe) (*SI Appendix*, Tables S2 and S4).

The observed soil temperature warming was primarily explained by an increase in air temperature during the nongrowing season and a decrease in wind speed during the growing season (adj. $R^2 = 0.59$, $P < 0.01$ in alpine meadow and adj. $R^2 = 0.53$, $P < 0.01$ in alpine steppe), rather than by air temperature during the growing season (*SI Appendix*, Table S3). The decreasing soil moisture was partly attributed to a lowering of the soil water table ($R^2 = 0.23$, $P < 0.05$ in alpine meadow and $R^2 = 0.39$, $P < 0.01$ in alpine steppe, respectively), which strongly positively correlated with an increase in the thickness of the active layer ($R^2 = 0.47$, $P < 0.01$

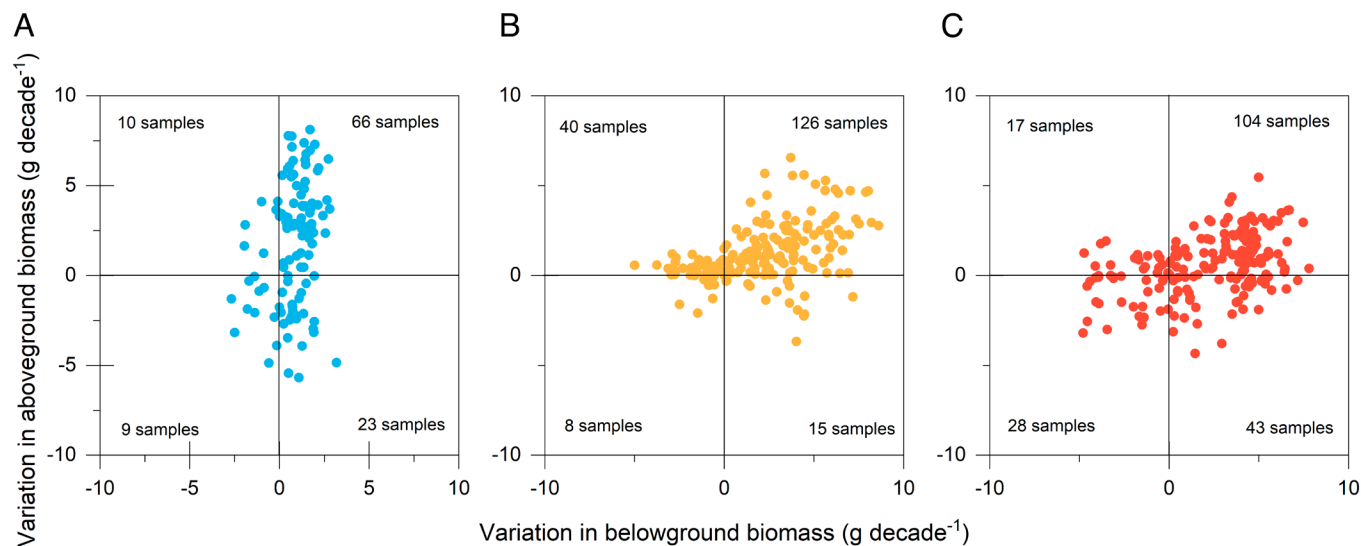


Fig. 3. Variation in above- and belowground biomass from 1995 to 2021. (A–C) variation in aboveground biomass versus variation in belowground biomass of the six studied plant species in the alpine wetlands (A, blue dot), eight studied plant species in the alpine meadows (B, orange dot), and 12 studied plant species in the alpine steppes (C, red dot). Each dot or sample represents an average of each studied species in a given year from 1995 to 2021.

in alpine meadow and $R^2 = 0.59$, $P < 0.01$ in alpine steppe) (SI Appendix, Fig. S10). This increase in active layer thickness (ALT) was well explained by an increase in air temperature, comparatively low soil moisture during the nongrowing season (18) and an exponential increase in snow cover during late spring and early summer on the Tibetan Plateau over the past five decades (18, 30).

Sensitivity of η to Climate Warming. Multiple regression analysis showed that soil temperature best explained the observed temporal variations in plot-level η within each vegetation type ($P < 0.01$; SI Appendix, Table S5). The partial derivative of η with respect to soil temperature increased from 0.008 in the first 13 y (1995 to 2007) to 0.030 $\text{decade}^{-1} \text{ } ^\circ\text{C}^{-1}$ in the most recent 13 y (2009 to 2021) in alpine wetlands (Fig. 4A). Conversely, the derivative decreased from -0.016 to $-0.041 \text{ } \text{decade}^{-1} \text{ } ^\circ\text{C}^{-1}$ in the alpine

meadow and from -0.021 to $-0.061 \text{ } \text{decade}^{-1} \text{ } ^\circ\text{C}^{-1}$ in the alpine steppe.

The sensitivity of plot-level η to soil temperature was significantly higher under dry soil conditions ($\delta > 0$) compared to wet soils ($\delta < 0$) in both alpine meadow and alpine steppe ($P < 0.01$), but there was no difference in alpine wetland ($P > 0.05$) (Fig. 4B). A Monte Carlo null experiment, assuming no change in moisture conditions, shows that the observed relationship between the partial derivative of η with respect to soil temperature and soil moisture is very unlikely to have occurred purely by chance ($P < 0.001$). This suggests that the impact of soil temperature on the temporal trend in η has become stronger under climate warming.

Importance of η on Model Fit and Temporal Predictions of SOC in Dynamic Vegetation Models. The biogeochemistry models (TEM 5.0, LPJ-GUESS 4.1, Coup Model 4.0, and ORCHIDEE-MICT 8.4.1) that rely on process-based equations could not fully

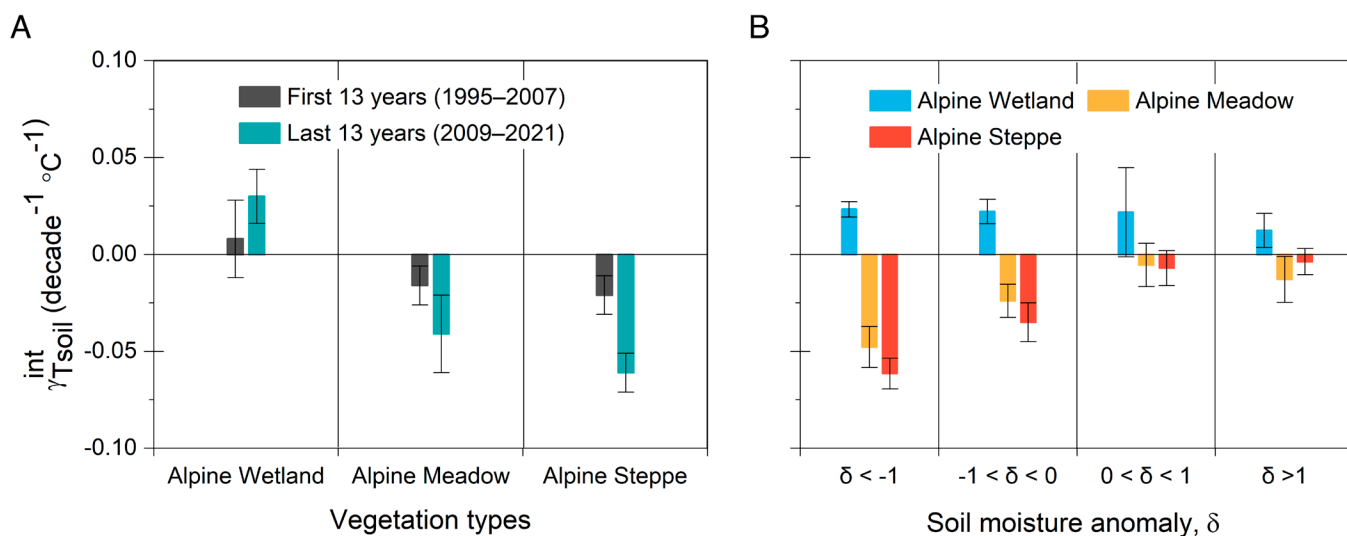


Fig. 4. Variation in the partial derivative of η with respect to soil temperature, $\gamma_{T_{\text{soil}}}^{\text{int}}$. (A) Partial derivative of estimated plot-level η with respect to soil temperature in the first 13 y (1995 to 2007) compared to the last 13 y (2009 to 2021) within three vegetation types. (B) The impact of soil moisture on the partial derivative of estimated plot-level η with respect to soil temperature. We grouped the 28-y data into four distinct bins of detrended soil moisture anomaly: very dry (δ less than -1), dry (δ between -1 and 0), wet (δ between 0 and 1), and very wet (δ greater than 1).

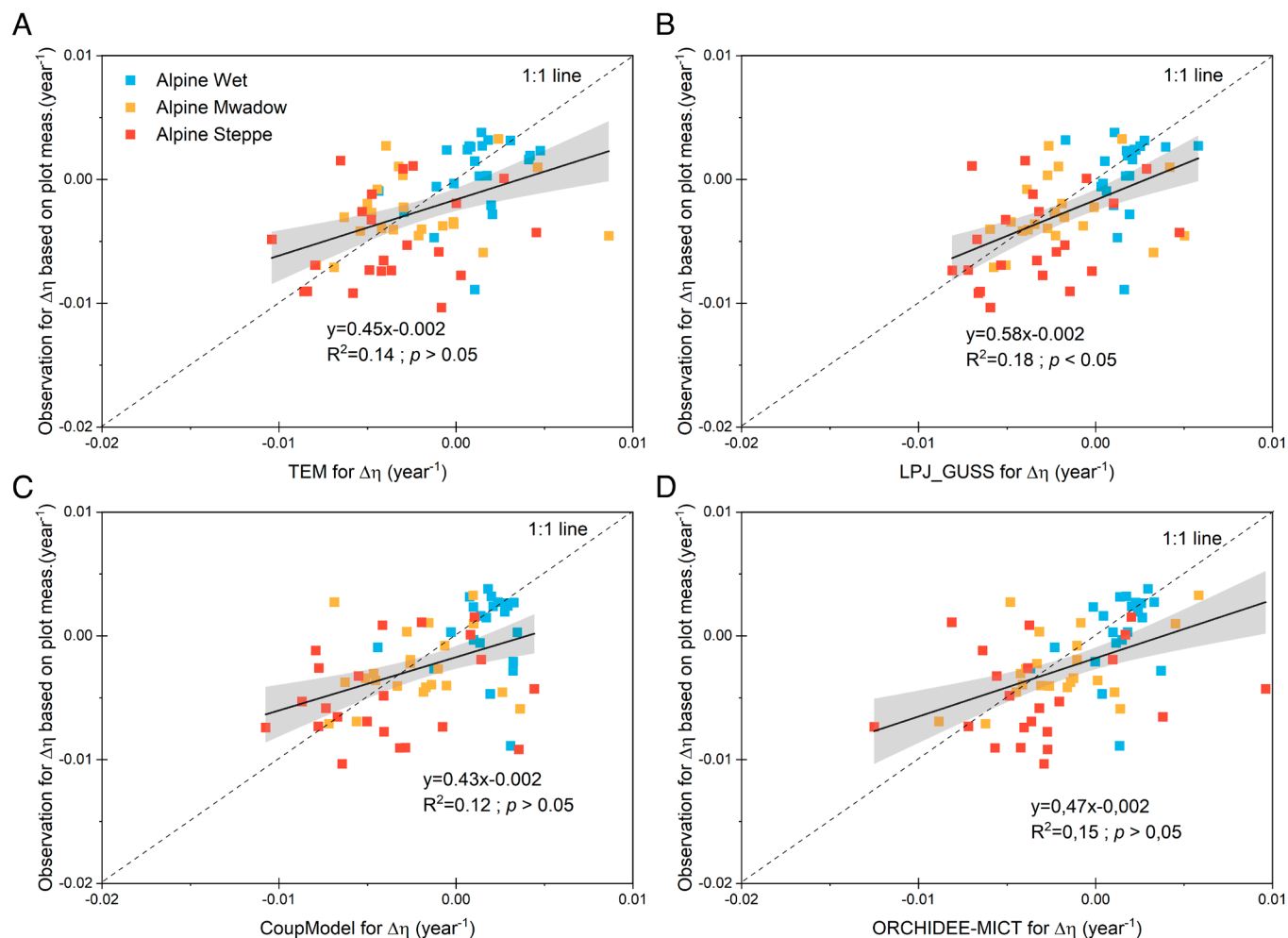


Fig. 5. Comparison of observed plot-level η values with estimated plot-level η using four commonly used dynamic vegetation models: TEM 5.0 (A) LPJ-GUESS 4.1 (B) Coup Model 4.0 (C) and ORCHIDEE-MICT 8.4.1 (D) Plot-level η variation in alpine wetland (blue square; $n = 22$), alpine meadow (orange line; $n = 22$), and alpine steppe (red square; $n = 22$) at a randomly chosen site (BLH station) from this study during 2009 to 2021. The baseline is the average η of 1995 to 2008. The black solid line is fitted by ordinary least squares linear regression and gray shading represents 95% CI. The dashed lines represent the 1:1 relationship.

reproduce the observed response of η to climate change over the last 27 y (Fig. 5 and *SI Appendix*, Fig. S11). They also did not capture the increased sensitivity of η to soil temperature *SI Appendix*, Fig. S12). All four models were only weakly correlated with the plot-level ($R^2 = 0.12$ to 0.18) (Fig. 5) and species-level observations ($R^2 = 0.04$ to 0.06) (*SI Appendix*, Fig. S11).

Discussion

Our study reveals significant shifts in biomass distribution between aboveground and belowground components across the Tibetan Plateau over the past three decades, highlighting the impact of climate warming on biomass distribution in alpine permafrost-affected ecosystems (18, 19). The observed changes in estimated plot-level η , with a 17% increase in alpine wetlands and notable decreases in alpine meadows (26.1%) and alpine steppes (48.2%), emphasize the variability and importance of these shifts across different vegetation types (Fig. 1C). The magnitude of these temporal shifts in η is comparable to the variation observed across different vegetation types. This emphasizes the profound impact of climate change on biomass distribution, underscoring the importance of considering these changes in ecological and climate models.

Previous studies have attributed temporal changes in η to shifts in plant species composition (26) and vegetation types (31), as well as direct environmental effects (32). Our results suggest that

soil temperature has been a major driver for changes in η across all vegetation types. In fact, the importance of soil temperature has been increasing as much as one and a half times more in alpine permafrost-affected ecosystems compared to Arctic tundra (1, 26, 33) and temperate grasslands (34–36). This highlights that alpine ecosystems underlain by permafrost are among the most susceptible regions with respect to their climate-sensitivity of biomass.

Soil temperature and water availability impact the temporal variation in η (26, 37, 38). However, other factors such as SOC status (39–41) and soil nutrient (33, 38) can also affect variation in η . Our findings indicate that, within the top 50 cm of soil, there has been a significant increase in both SOC and total nitrogen stocks across the three vegetation types since 1995 (*SI Appendix*, Table S6). Despite this, our analysis reveals no direct relationship between η and the stocks of SOC and total nitrogen ($P > 0.05$) (*SI Appendix*, Table S5).

In contrast to soil nutrients, soil moisture seems to have impacted the direction and strength of the relationship between η and soil temperature (26, 37). Over the last three decades, there has been no significant change in total precipitation during summer, but heavy precipitation events have increased ($P < 0.01$) (18). The soil moisture content of alpine wetlands has remained constant at $\sim 26\%$ ($P > 0.05$), whereas the mean soil moisture content of alpine meadows and alpine steppes has significantly decreased from 15.3% to 12.2% and from 12.7 to 7.5%, respectively ($P < 0.01$)

(SI Appendix, Fig. S7). These results suggest an important role of soil moisture in modulating the effect of soil temperature on η on the Tibetan Plateau.

Previous studies have shown that changes in plant growth, abundance, and community composition in response to climate change had a significant impact on temporal trends in η (42, 43). However, our analysis showed that changes in species composition have not significantly contributed to the decreases in η in alpine meadows and steppes. Since 1995, no significant species changes occurred in alpine wetland, and only two and four species changes were recorded in alpine meadow and alpine steppe ecosystems, respectively (19, 44). When excluding these species, the mean values of η remained within the 95% CI of the original analysis including all species and showed a consistent long-term decline in η . This suggests that the increases in η in alpine wetlands and the decreases in η in alpine meadows and alpine steppes are unlikely to have resulted from changes in species richness or community composition.

While the temporal variation in species richness does not appear to be the driving factor behind the changes in η over time, differences in species abundance at various sites do partially account for the multiple peaks observed for the three-dimensional interactions between soil temperature, moisture, and η (Fig. 2 and SI Appendix, Fig. S4). For instance, the abundance of *Stipa purpurea* in alpine meadows is notably higher at some sites (BLH, KXL, QML, and TM), with over 73 individuals per square meter, compared to less than 15 individuals per square meter at other sites (HSX, TSH, and XDT) (44).

Extreme warming or extreme drought might also affect the above- versus belowground plant biomass distribution, as high temperature and drought limit photosynthesis (34, 45, 46) and stimulate closure of leaf stomata (46, 47). Our results show that the two largest anomalies in estimated plot-level η occurred under warm and dry summer conditions in 1998 and 2014, with a mean June to August air temperature $>15^\circ\text{C}$ and total precipitation <82 mm (SI Appendix, Table S7). In these years, temperature and precipitation were more than 25% higher/lower compared to the 1995 to 2021 means and η decreased by a factor of 0.04 to 0.12 in the three vegetation types. This matches previous studies showing that extreme warming and drought stimulates shifts toward an increased proportion of belowground biomass relative to aboveground biomass in tundra ecosystems (21, 48, 49). Although η substantially decreased in some plant species in the two extreme years, this did not affect the robustness of the relationship between (plot-level) η and soil temperature. While we found a slight increase in the partial effect of soil temperature on η after excluding the anomalous years 1998 and 2014, the results remained within the 90% CI of the original analysis (SI Appendix, Fig. S13), showing that the inferred increases or decreases in the effect of soil temperature on η are not driven by outlier years.

The four process-based biogeochemical models failed to accurately reflect the observed changes in η based on measurements of the dominant species in each plot (estimated plot-level η ; see SI Appendix, Fig. S11) as well as actual plot-level measurements (Fig. 5) in response to changes in climate. This discrepancy highlights significant limitations in the current models' ability to predict temporal biomass changes under varying climatic conditions. However, it is important to note that this mismatch between model predictions and our observations may be partly attributed to our methodology, which primarily focused on biomass observations from dominant species, rather than comprehensive data from entire plots. Ecological studies often find that whole plots are less reactive to environmental changes than individual species (50, 51). In our research, we identified dominant plant species

based on aboveground characteristics, such as species abundance and coverage, but did not consider belowground traits. This approach effectively captured the aboveground biomass traits at both species and plot levels and the distribution of biomass between above- and belowground at the species level. However, its representation of belowground biomass at the plot-level warrants cautious interpretation. This limitation stems from the potential for nondominant species, which may have a limited aboveground presence at the ecosystem scale, to nonetheless contribute substantially to the belowground biomass. Although we aimed to encompass a diverse array of species, our data may not fully capture total belowground biomass because our estimated plot-level η was calculated by summing the species-level measurements of the dominant species. However, the direct plot-level measures show the same trends (SI Appendix, Figs. S14–S16).

Our method for collecting belowground biomass was confined to a depth of 0 to 50 cm. This approach likely leads to an underestimation of the actual belowground biomass for individual species, particularly for those with root systems extending beyond 50 cm (19, 44). Considering the tendency of deep-rooted plants to grow deeper in search of nutrients, like nitrogen, increasingly released from thawing permafrost due to climate warming over the past three decades (44), our methodology may not entirely capture the actual plot-level belowground biomass and the overall η variation. Despite these limitations, the discrepancies observed between model predictions and actual changes in η provide important insights. These findings highlight areas where models can be refined and improved for greater accuracy in representing ecological dynamics.

Conclusion

Our study provides important insights into the multidecadal variation of the above- and belowground biomass ratio (η) in permafrost-affected ecosystems of the Tibetan Plateau under climate warming. Our findings indicate that the temporal variation of estimated plot-level η varies significantly with vegetation types, with η increasing in alpine wetlands and decreasing in alpine meadows and alpine steppes. Temporal variation of η was predominantly driven by soil temperature changes, and the sensitivity of η to soil temperature has increased by a factor of 3.1 ± 0.3 over the past 27 y. This highlights the urgent need for effective measures to mitigate the impacts of climate change on permafrost-affected ecosystems.

Additionally, in alpine meadows and alpine steppes, we observed that the sensitivity of η to temperature was more pronounced under high soil moisture conditions, highlighting the critical role of soil moisture in modulating the sensitivity of η to soil temperature in these ecosystems. However, in alpine wetlands where water availability is not limiting, no significant influence of soil moisture on the soil temperature sensitivity of η was observed. Last, our study emphasizes the limitations of current process-based biogeochemistry models in capturing the responses of η to climate change and the increased sensitivity of η to soil temperature. Incorporating the responses of η to changing soil conditions in these models holds potential to improve projections of SOC pools and turnover under different climate-change scenarios.

Materials and Methods

In the following, we describe how we 1) compiled and quality-checked η values (above- to belowground biomass ratio of plants) at the species level along with meteorological data from 3,013 plots and 26,337 species-specific measurements; 2) delineated η values; 3) analyzed the data; 4) integrated the species

measurements to estimate plot-level η values, and 5) used the output of four dynamic vegetation models to test the extent to which these models capture observed changes in η at the species-level and plot-level as well as the sensitivity of η to soil temperature.

Environmental Data Compilation. The location of the eight sites is shown in Fig. 1A. Meteorological data (air temperature, air humidity, wind speed, net radiation at two meters aboveground, precipitation from May to September, soil temperature and moisture at 30 cm depth) for the sites of Xida Tan (XDT), Liangdaohe (LDH), and Tianshui Hai (TSH) were downloaded from weather station data from the National Cryosphere Desert Data Center, China (<http://www.ncdc.ac.cn/portal/>); those for the sites of Huangshi Xia (HSX) and Qumalai (QML) were downloaded from the Meteorological Data Service Center, China (<http://data.cma.cn/>); and those for the sites of Beilu He (BLH), Tumen (TM), and Kaixin Ling (KXL) were provided by the State Key Laboratory of Frozen Soil Engineering, China (<http://sklfse.nieer.ac.cn/>). We used a hierarchical data fill method (52, 53) to fill data gaps. To generate a dataset with consistent time resolution (yearly growing season) of meteorological data, soil temperature, soil moisture, and the ratio between above- and belowground biomass (η), we averaged daily air temperature, total precipitation, soil temperature, and soil moisture in the growing season (from 1 May to 30 September) and nongrowing season (from 1 October to 30 April) at each site. To approximate the effect of permafrost variation on η under climate warming, we used the maximum ALT in late autumn in each vegetation type and site, which was identified by the maximum depth at which the 0 °C isotherm (soil temperature) occurs in a specific year (54).

Plant Biomass Data Compilation. At each site, located within a 17-km radius of the weather station, we selected two or three dominant vegetation types—alpine wetland, alpine meadow, and alpine steppe. We chose these types because they represent the Tibetan Plateau’s permafrost region well, as their combined normalized difference vegetation index (NDVI) accounts for 61.3% of the total NDVI sum for the entire study area (42). These vegetation types are separated by distances ranging from 3 to 12 kilometers, following a gradient of increasing aridity (55).

In the Tibetan Plateau region, the alpine wetland is considered particularly vulnerable to climate impacts (56), occupying about 5.7% of the land area and containing more than 33% of the area’s carbon stock (42). The average annual soil temperature is approximately –4.6 °C, with soil moisture levels around 26%. During the summer, water typically remains in the low-lying areas between plants (56). Around 65% of the area is covered by vegetation, with species richness being relatively uniform across the area. The landscape is primarily dominated by species such as *Kobresia*, *Delphinium*, and *Heteropappus*. Additionally, areas of exposed soil are generally covered with moss, contributing to the unique ecological makeup and function of these wetlands in carbon storage and ecosystem stability (19).

The alpine meadow, covering one-third of the Tibetan Plateau, exhibits soil temperature and moisture levels intermediate between those of the alpine wetland and alpine steppe. Plant cover in meadows varies from 35% to 52% (42), with *Kobresia*, *Androsace*, and *Heteropappus* as the dominant species.

The alpine steppe, which makes up about half of the Tibetan area, is identified as one of the most critical vegetation types (56). It has an average colder annual soil temperature of –7.8 °C and soil moisture levels consistently below 13% (57). Despite having sparse vegetation with less than 30% plant cover, it features high species richness with low abundance of individual species (44), including *Carex*, *Kobresia*, and *Allium*, among others.

For each vegetation type, we measured the soil temperature profile using constantan–copper thermocouples at 10 cm intervals down to a depth of 500 cm. The temperature profile was also used to monitor the maximum ALT. Centered around the soil temperature borehole (soil temperature measurement profile), we defined a 100 m transect along which we randomly placed five pairs of one square meter plots. We selected one side of the transect for biomass collection of individual species and soil property measurements (five plots) and the opposite side for collecting plot-level biomass samples as a control (another five plots). This sampling of five plot pairs minimizes the occasional presence of small animal dung or disturbances, which could randomly occur within the plot area. To mitigate the impact of seasonal variations due to phenological changes such as blooming and seeding, we conducted annual biomass measurements from

1995 to 2021 between the end of August and early September, when all species were at full maturity.

Individual Species Biomass Collection. Initially, for each plot, we captured one to three high-resolution photographs (300 × 300 dpi) from a vertical perspective using a Nikon camera. These images were used to quantify the abundance of each species, which were later analyzed at the Lanzhou City lab. We manually measured the abundance of each species within the plot, applying a grid to the photographs and conducting five independent assessments. The mean abundance of each species was then calculated to represent its prevalence in the plot.

Species identities, plant coverage (using Tetracam’s LCD-equipped agricultural digital camera), plant height, landscape type, soil surface drainage characteristics, and erosion status were directly monitored and recorded in the field.

We identified key species at each site: 6 to 8 in alpine wetlands, 8 to 10 in alpine meadows, and 8 to 12 in alpine steppes. These species represented the dominant plants at the sites and collectively constitute over 57% of plant coverage and 59% of the average aboveground biomass (SI Appendix, Table S8). Within the plots, we randomly selected and marked four mature plants of each key species (target plants) with permanent markers. Subsequently, the aboveground and belowground parts of target plants were harvested using a specialized soil sample drill (devised by Professor Shunji Kanie’s group at Hokkaido University). This soil drill was designed to ensure that the aboveground and belowground sections of the sampled plant were extracted as a single, intact unit, maintaining their natural connection without any separation. The drill has been successfully tested in a previous experiment showing that the majority of roots were concentrated within specific diameters and depths: more than 92% within a 12 cm diameter in wetlands, and over 97% within a 6 cm diameter in steppes and meadows, with more than 82% of roots across all vegetation types located within the top 50 cm of soil (19). Accordingly, we employed a 15 cm diameter drill for wetlands and a 10 cm diameter for steppes and meadows, collecting soil cores down to a depth of 50 cm.

The harvested plant parts (above- and belowground biomass of the target plant and other plants) and soil cores were horizontally packed in ventilated canvas bags and transported to the laboratory. There, they were gently rinsed in slowly flowing water to separate the soil from the plant biomass. The cleaned samples were air-dried for half an hour.

We separated the target plant’s biomass from that of other plants, guided by markers previously placed on the aboveground portion of the target plant in the field. This segregation process ensured that the biomass of the target plant was completely separated from other plants. Above- and belowground components of the target plant were then separated. Finally, both aboveground and belowground biomass samples were dried in an oven at 75 ± 2 °C for 72 h. After drying, the biomass was weighed to calculate the average mass value for each plant species.

The Ratio between Above- and Belowground Biomass, η . The η of each species (η_{species}) was calculated by dividing the species-specific aboveground biomass by the belowground biomass:

$$\eta_{\text{species}} = \frac{\text{Above ground biomass}_{\text{specific—species}}}{\text{Below ground biomass}_{\text{specific—species}}}, \quad [1]$$

η at the plot-level (η_{plot}) was calculated by the weighted mean value of η_{species} for major species in the plot:

$$\eta_{\text{plot}} = \frac{\eta_{\text{species},1} \times \omega_{\text{species},1} + \eta_{\text{species},2} \times \omega_{\text{species},2} + \dots + \eta_{\text{species},n} \times \omega_{\text{species},n}}{\omega_{\text{species},1} + \omega_{\text{species},2} + \dots + \omega_{\text{species},n}}, \quad [2]$$

$$\omega_{\text{species},i} = \frac{\text{Population of specific—species}_i}{\text{Sum population of specific—species within each plot}}. \quad [3]$$

Plot Level Biomass Collection (Control). To compare our biomass data from plant samples with plot-level biomass estimated from measurements of all species, we collected comprehensive above- and belowground biomass data from an additional five plots at each corresponding site every 2 y. Aboveground biomass was harvested by cutting all plant material above the ground at a height of negative 2 cm. This material was then placed in paper bags and transported to

the laboratory. Upon arrival at the laboratory, any soil particles adhering to the plant samples were carefully removed. The plant material was then dried at $75 \pm 2^\circ\text{C}$ for 72 h to determine the aboveground biomass.

For the belowground biomass, we initially used a manual excavation method, digging a one square meter pit to a depth of 50 cm from 1995 to 2007. In 2008, we shifted to a more efficient soil coring technique, utilizing a specialized soil-sample drilling device with a 15 cm diameter. This device, designed by the State Key Laboratory of Frozen Soil Engineering in China, allowed for four replicates to be taken from each plot. The soil cores were sieved in the field through a 5×5 mm mesh and then placed in ventilated canvas bags. In the laboratory, these samples were gently washed in slow-flowing water to separate the biomass from the soil. Following this process, the biomass was dried at $75 \pm 2^\circ\text{C}$ for 72 h and then weighed to calculate the belowground biomass. The corresponding plot-level η (actual plot-level η) was determined by dividing the total plot-level aboveground biomass by the total plot-level belowground biomass.

Furthermore, we compared plot-level η obtained from the direct measurements (actual plot-level η) with estimated plot-level η measures based on the species-level measurements across the three vegetation types on the Tibetan Plateau. Linear regression between the two metrics yielded R^2 values from 0.43 to 0.59 in alpine wetlands, 0.43 to 0.57 in alpine meadows, and 0.29 to 0.51 in alpine steppes, respectively (SI Appendix, Figs. S14–S16).

Data Quality, Spatial Autocorrelation, and Temporal Trend. We conducted a multistep hierarchical data quality test following Essington et al. (58) to objectively identify outliers. Subsequently, we tested for spatial autocorrelation as few locations were relatively close to each other. Finally, we assessed whether different periods during the observation years influenced the overall trends in species' biomass, plot biomass, and climate variables. Following the methods of O'Reilly et al. (59), we defined yearly anomalies of each parameter at each site as the difference between the yearly mean value and the overall mean value. Please see SI Appendix, Supplementary Methods for details.

Characterizing Temporal Trends in η and Climate Variables. For each site, we calculated the mean annual values of η at the species and plot levels within each vegetation type. The mean values of climate variables listed in SI Appendix, Table S6 were calculated for the entire year, the growing season, and the nongrowing season. Soil moisture was averaged across the growing season.

We excluded aforementioned datasets that spanned less than 15 y (SI Appendix, Table S9). We then tested for temporal trends in all variables using linear regression and the Mann–Kendall test. To account for possible nonlinear temporal trends, we also ran GAMMs (60); see below section for details on parameters. All predictors and η values were z-scaled before analysis.

Identifying the Predictors for Temporal Trends in η . Within each vegetation type, we ran GAMMs to identify the possible climate drivers of temporal variation in estimated plot-level η (package of *gam4* in R 4.1). GAMMs fit a nonlinear or linear function between the predictor variables and the response variable η (60, 61). We stepwise entered all the climate variables by linear or smoothing functions against η (dependent variable). In those GAMMs, we used the *gam4* function in *mgcv* package to fit smoothing terms by the default thin plate spline technique. *Gamm4* uses penalized regression splines of moderate rank for the smoothing function (61). We limited this analysis to data since 1995 and included all three vegetation types with species and plot level data in the specific period. For all models, we used a normal error distribution.

To account for the dependent nature of the repeated measurements over time within each vegetation type, we further allowed the slope and intercept to vary randomly by site and plant species followed by Québec Centre for Biodiversity Science R WORKSHOP SERIES (<https://r.qcbs.ca/workshop08/book-en/introduction-to-generalized-additive-mixed-models-gamms.html>). We selected the model with the lowest Akaike information criterion (AIC). The results were assessed by the adjusted R^2 and P value (P), with a significance level < 0.05 and a confidence level of 95%.

Additionally, we ran convergent cross-mapping (CCM) to validate the reasonability of the predictors identified in above GAMMs, as well as to identify the possible time lag between those predictors and η temporal variation (package of *mgcv* in R 4.1). In the CCM, the optimal value of the embedding dimension (E) was 2, estimated by the function of the SSR pred boot (60).

Contribution of Each Predictor in η Temporal Trends. Although the GAMMs were effective in selecting predictors and quantifying their overall contribution (deviance explained) to the observed temporal change in η , they could not quantify the contributions of specific predictors. Therefore, we additionally used multiple linear regression to quantify the contribution of each predictor.

Quantifying the Sensitivity of η to Climate Change. To calculate the sensitivity of η to interannual climate variability, we used the slope of estimated plot-level η with respect to soil temperature in the earliest time window (the first 13 y, 1995 to 2007) and the most recent time window (the past 13 y, 2009 to 2021) using general linear regression and then compared the slopes between these two time windows, which were derived from fully independent subsets of the data.

The slope of η with respect to soil temperature in general linear regression may not truly reflect the change in η in response to interannual soil temperature variation, due to the indirect effect of soil temperature with other climate variables, such as soil moisture, precipitation, and solar radiation during the growing season (18). To better isolate the individual role of soil temperature, we performed a multilinear regression with all mentioned variables against η and compared the partial regression slope of η to soil temperature within the same time windows.

Characterizing the Robustness of the Relationship between η and Soil Temperature under Different Soil Moisture Levels. To quantify the effect of soil moisture (yearly scale) on the partial derivative of η in response to soil temperature, we compared the partial derivative sensitivity of η to soil temperature under four soil moisture conditions. First, the annual partial derivative η in relation to soil temperature was calculated by a 10-y moving window from 1995 to 2021, and then the partial derivative η to soil temperature dataset was grouped into four distinct bins, defined by yearly soil moisture within each vegetation type, then grouping the data into less than -1 , between -1 and 0 , between 0 and 1 , and greater than 1 SD (σ) (Eq. 4). We calculate the partial derivative sensitivity of η to soil temperature within each bin of normalized soil moisture and assessed the differences in the partial derivative sensitivity of η to soil temperature under four different soil moisture conditions.

$$\sigma_i = \frac{M_{\text{soil}_i} - M_{\text{soil}_{\text{mean}}}}{\text{Std}_{M_{\text{soil}}}} \quad [4]$$

Here, M_{soil_i} is the soil moisture at 30 cm in year i , and $M_{\text{soil}_{\text{mean}}}$ and $\text{Std}_{M_{\text{soil}}}$ are the average and SD of the soil moisture from 2004 to 2021, respectively. An alternative of splitting the soil moisture dataset into eight bins based on σ (less than -1.5 , between -1.5 and -1 , between -1 and -0.5 , between -0.5 and 0 , between 0 and 0.5 , between 0.5 and 1 , between 1 and 1.5 , and greater than 1.5) did not qualitatively change the result.

Ecosystem Model Projections of η and SOC. To assess how well various models capture the trends in η , we employed four dynamic vegetation models: the Terrestrial Ecosystem Model 5.0 (TEM) (62), LPJ-GUESS 4.1 (63), the CoupModel 4.0 (28), and ORCHIDEE-MICT (8.4.1) (64). These models were used to simulate annual variations in η and SOC across four sites on the Tibetan Plateau (BLH, HSX, QML, XDT), each with over 25 y of meteorological data.

For the simulations, we selected a spatial resolution of 0.5° by 0.5° and pinpointed the grid cell center nearest to each study site. The extent of each vegetation type within these cells was calculated by averaging high-resolution vegetation type maps (10 m by 10 m) spanning from 2018 to 2021 (62). We sourced climate variables and soil property data from the local permafrost observation stations and obtained vegetation type and plant trait data from the State Key Laboratory of Frozen Soil Engineering, China, which can be accessed online (<http://sklfse.nieer.ac.cn/>). We handled any gaps in the climate data by employing methods outlined by Ding et al. (52) and Du et al. (53).

A notable limitation was encountered with the LPJ-GUESS 4.1 model, which only simulated SOC up to a depth of 150 cm, omitting the deeper layer between 151 and 300 cm. To align this model's output with the others, we interpolated the missing layer's SOC values using the mean values derived from TEM 5.0, CoupModel 4.0, and ORCHIDEE-MICT 8.4.1. Additionally, we ensured consistency in training across all models by using the same set of meteorological data from the period 1990 to 2010.

Since these four models have only one or two plant function types (PFTs) to represent natural grassland, they do not differentiate between different plant species in the alpine wetlands, alpine meadows, and alpine steppes. In order to better represent the plants observed in these vegetation types, we calibrated the plant growth rate, photosynthetic efficiency, and water use efficiency in the grassland PFT based on observed plant traits (63), such as root length, leaf area index, leaf albedo, and physiological parameters (64, 65), such as maximum rubisco-limited potential photosynthetic capacity (V_{cmax}).

We initialized soil properties such as pH value, SOC content, and soil bulk density, as well as permafrost characteristics such as ALT and ice content (excluded in LPJ-GUESS 4.1), specific to each vegetation type. For the alpine wetlands, the TEM 5.0 and Coup Model 4.0 were parameterized using the plant functional type of wet tundra, and we ran the models using local climate variables, soil properties, and permafrost characteristics specific to each site. We optimized the parameters with an iterative model simulation (62, 64) to minimize the differences between the simulations and observations. Once the models were stable, they were used to mimic the aboveground biomass, belowground biomass, and SOC for the specific site from 2011 to 2021.

Data, Materials, and Software Availability. All sites of soil properties, plant traits data, and R code used for the analysis used in this manuscript are publicly available from ZENODO: <https://zenodo.org/records/11218337> (66).

ACKNOWLEDGMENTS. Many thanks to PNAS reviewers for very helpful comments and recommendations. B.E. and H.Y. were supported by the Danish National Research Foundation (CENPERM DNR 100), Q.W. was supported by the National Natural Science Foundation of China (42230512), C.M.Z. was funded by the Ambizione Grant PZ00P3_193646, and Q.Z. was supported by the Reducing Uncertainties in Biogeochemical Interactions through Synthesis and Computation

Scientific Focus Area, Office of Biological and Environmental Research of the U.S. Department of Energy. In addition, H.Y. was supported by the Chinese Academy of Sciences (YJKYQ20190012 and E229060201) and State Key Laboratory of Frozen Soil Engineering (SKLFSE-ZT-202111), D.C. was supported by the Strategic Research Area Modelling the Regional and Global Earth system and Biodiversity and Ecosystem services in a Changing Climate, funded by the Swedish government.

Author affiliations: ^aState Key Laboratory of Frozen Soil Engineering, Beilu/He Observation and Research Station on Tibetan Plateau, Northwest Institute of Eco-Environment and Resources, Chinese Academy of Sciences, Lanzhou 730000, Gansu, China; ^bKey Laboratory of Cryospheric Science and Frozen Soil Engineering, Northwest Institute of Eco-Environment and Resources, Chinese Academy of Sciences, Lanzhou 730000, Gansu, China; ^cCenter for Permafrost, Department of Geosciences and Natural Resource Management, University of Copenhagen, Copenhagen DK1350, Denmark; ^dDepartment of Earth, Atmospheric, and Planetary Sciences, Purdue University, West Lafayette, IN 47906; ^eIPSL-Laboratoire des Sciences du Climat et de l'Environnement, Commissariat à l'Énergie Atomique et aux Énergies Alternatives CNRS UVSQ Université ParisSaclay, Centre d'Études Orme des Merisiers, Gif sur Yvette 91191, France; ^fClimate Sciences Department, Climate and Ecosystem Sciences Division, Lawrence Berkeley National Laboratory, Berkeley, CA 94720; ^gDepartment of Earth Sciences, University of Gothenburg, Gothenburg 405 30, Sweden; ^hInstitute of Integrative Biology, Eidgenössische Technische Hochschule Zurich (Swiss Federal Institute of Technology), Zurich 168092, Switzerland; ⁱDepartment of Biology, Terrestrial Ecology and Center of Volatile Interactions, University of Copenhagen, Copenhagen DK-2100, Denmark; ^jDepartment of Physical Geography and Ecosystem Science, Lund University, Lund SE-22236, Sweden; ^kInstitute for Global Innovation and Development, East China Normal University, Shanghai 200062, China; ^lDepartment of Ecology, Evolution and Marine Biology, University of California, Santa Barbara, CA 93108; ^mDepartment of Geography, The University of Hong Kong, Hong Kong 999077, Special Administrative Region of China; ⁿInstitute for Climate and Carbon Neutrality, The University of Hong Kong, Hong Kong 999077, Special Administrative Region of China; ^oKey laboratory of oil and gas resources exploration and development in Gansu province, Northwest Institute of Eco-Environment and Resources, Chinese Academy of Sciences, Lanzhou 730000, China; ^pNiels Bohr Institute, University of Copenhagen, Copenhagen DK1350, Denmark; and ^qDepartment of Biology and Graduate Degree Program in Ecology, Colorado State University, Fort Collins, CO 80523

- A. D. Bjorkman *et al.*, Plant functional trait change across a warming tundra biome. *Nature* **562**, 57–62 (2018), 10.1038/s41586-018-0563-7.
- R. D. Hollister, P. J. Webber, C. E. Tweedie, The response of Alaskan arctic tundra to experimental warming: Differences between short- and long-term responses. *Global Change Biol.* **11**, 525–536 (2005), 10.1111/j.1365-2486.2005.00926.x.
- K. A. Heilman *et al.*, Ecological forecasting of tree growth: Regional fusion of tree-ring and forest inventory data to quantify drivers and characterize uncertainty. *Global Change Biol.* **28**, 2442–2460 (2022), 10.1111/gcb.16038.
- F. S. Chapin *et al.*, Role of land-surface changes in Arctic summer warming. *Science* **310**, 657–660 (2005), 10.1126/science.1117368.
- I. H. Myers-Smith *et al.*, Complexity revealed in the greening of the Arctic. *Nat. Clim. Change* **10**, 106–117 (2020), 10.1038/s41558-019-0688-1.
- F. Keuper *et al.*, Carbon loss from northern circumpolar permafrost soils amplified by rhizosphere priming. *Nat. Geosci.* **13**, 560–565 (2020), 10.1038/s41561-020-0607-0.
- B. Wild *et al.*, Input of easily available organic C and N stimulates microbial decomposition of soil organic matter in arctic permafrost soil. *Soil Biol. Biochem.* **75**, 143–151 (2014), 10.1016/j.soilbio.2014.04.014.
- L. E. Street *et al.*, Plant carbon allocation drives turnover of old soil organic matter in permafrost tundra soils. *Global Change Biol.* **26**, 4559–4571 (2020), 10.1111/gcb.15134.
- C. D. Koven, D. M. Lawrence, W. J. Riley, Permafrost carbon—climate feedback is sensitive to deep soil carbon decomposability but not deep soil nitrogen dynamics. *Proc. Natl. Acad. Sci. U.S.A.* **112**, 3752–3757 (2015), 10.1073/pnas.1415123112.
- A. Ledo *et al.*, Tree size and climatic water deficit control root to shoot ratio in individual trees globally. *New Phytol.* **217**, 8–11 (2018), 10.1111/nph.14863.
- U. S. Bhatt *et al.*, Recent declines in warming and vegetation greening trends over pan-Arctic tundra. *Remote Sens.* **5**, 4229–4254 (2013), 10.3390/rs5094229.
- K. C. Guay *et al.*, Vegetation productivity patterns at high northern latitudes: A multi-sensor satellite data assessment. *Global Change Biol.* **20**, 3147–3158 (2014), 10.1111/gcb.12647.
- T. V. Colodetti *et al.*, The management of orthotropic stems modulates the photosynthetic performance and biomass allocation of productive plants of Arabica coffee. *Rev. Ceres* **67**, 454–463 (2020), 10.1590/0034-737X202067060005.
- R. E. Hewitt, D. L. Taylor, H. Genet, A. D. McGuire, M. C. Mack, Below-ground plant traits influence tundra plant acquisition of newly thawed permafrost nitrogen. *J. Ecol.* **107**, 950–962 (2019), 10.1111/1365-2745.13062.
- K. Prach, L. R. Walker, *Comparative Plant Succession among Terrestrial Biomes of the World* (Cambridge University Press, 2020).
- V. G. Salmon *et al.*, Adding depth to our understanding of nitrogen dynamics in permafrost soils. *J. Geophys. Res.-Biogeophys.* **123**, 2497–2512 (2018), 10.1029/2018JG004518.
- E. P. Pedersen, B. Elberling, A. Michelsen, Foraging deeply: Depth-specific plant nitrogen uptake in response to climate-induced N-release and permafrost thaw in the High Arctic. *Global Change Biol.* **26**, 6523–6536 (2020), 10.1111/gcb.15306.
- H. Yun *et al.*, Warming and increased respiration have transformed an alpine steppe ecosystem on the Tibetan Plateau from a carbon dioxide sink into a source. *J. Geophys. Res.-Biogeophys.* **127**, e2021JG006406 (2022), 10.1029/2021JG006406.
- H. Liu *et al.*, Phenological mismatches between above- and belowground plant responses to climate warming. *Nat. Clim. Change* **12**, 97–102 (2022), 10.1038/s41558-021-01244-x.
- G. Blume-Werry *et al.*, Proportion of fine roots, but not plant biomass allocation below ground, increases with elevation in arctic tundra. *J. Veg. Sci.* **29**, 226–235 (2018), 10.1111/jvs.12605.
- H. Poorter *et al.*, Biomass allocation to leaves, stems and roots: meta-analyses of interspecific variation and environmental control. *New Phytol.* **193**, 30–50 (2012), 10.1111/j.1469-8137.2011.03952.x.
- R. G. Pearson *et al.*, Shifts in Arctic vegetation and associated feedbacks under climate change. *Nat. Clim. Change* **3**, 673–677 (2013), 10.1038/nclimate1858.
- S. Bam, J. P. Ott, J. L. Butler, L. Xu, Belowground mechanism reveals climate change impacts on invasive clonal plant establishment. *Sci. Rep.* **12**, 2860 (2022), 10.1038/s41598-022-06918-w.
- C. Nilsson, R. Jansson, L. Kuglerová, L. Lind, L. Ström, Boreal riparian vegetation under climate change. *Ecosystems* **16**, 401–410 (2013), 10.1007/s10021-012-9622-3.
- G. Ottaviani *et al.*, The neglected belowground dimension of plant dominance. *Trends Ecol. Evol.* **35**, 763–766 (2020), 10.1016/j.tree.2020.06.006.
- H. Ma *et al.*, The global distribution and environmental drivers of aboveground versus belowground plant biomass. *Nat. Ecol. Evol.* **5**, 1110–1122 (2021), 10.1038/s41559-021-01485-1.
- Q. Zhuang *et al.*, Carbon dynamics of terrestrial ecosystems on the Tibetan Plateau during the 20th century: An analysis with a process-based biogeochemical model. *Global Ecol. Biogeogr.* **19**, 649–662 (2010), 10.1111/j.1466-8238.2010.00559.x.
- M. H. Madani, P. E. Jansson, *Infiltration into Soil Profile (Coup Model Tutorial)* (Royal Institute of Technology, Stockholm, Sweden, 2014).
- Y. Qi, W. Wei, C. Chen, L. Chen, Plant root-shoot biomass allocation over diverse biomes: A global synthesis. *Global Ecol. Conserv.* **18**, e00606 (2019), 10.1016/j.gecco.
- T. A. Ehlers *et al.*, Past, present, and future geo-biosphere interactions on the Tibetan Plateau and implications for permafrost. *Earth-Sci. Rev.* **234**, 104197 (2022), 10.1016/j.earscirev.2022.104197.
- K. T. Vashum, S. Jayakumar, Methods to estimate above-ground biomass and carbon stock in natural forests—A review. *J. Ecosyst. Ecogr.* **2**, 1–7 (2012), 10.4172/2157-7625.1000116.
- J. M. O. Scurlock, K. Johnson, R. J. Olson, Estimating net primary productivity from grassland biomass dynamics measurements. *Global Change Biol.* **8**, 736–753 (2002), 10.1046/j.1365-2486.2002.00512.x.
- S. C. Elmendorf *et al.*, Plot-scale evidence of tundra vegetation change and links to recent summer warming. *Nat. Clim. Change* **2**, 453–457 (2012), 10.1038/nclimate1465.
- M. G. Tjoelker, J. M. Craine, D. Wedin, P. B. Reich, D. Tilman, Linking leaf and root trait syndromes among 39 grassland and savannah species. *New Phytol.* **167**, 493–508 (2005), 10.1111/j.1469-8137.2005.01428.x.
- R. B. Jackson, H. A. Mooney, E. D. Schulze, A global budget for fine root biomass, surface area, and nutrient contents. *Proc. Natl. Acad. Sci. USA* **94**, 7362–7366 (1997).
- I. Husakova, J. Weiner, Z. Munzbergova, Species traits and shoot-root biomass allocation in 20 dry-grassland species. *J. Plant Ecol.* **11**, 273–285 (2018), 10.1093/jpe/rtw143.
- C. M. Iversen *et al.*, The unseen iceberg: Plant roots in Arctic tundra. *New Phytol.* **205**, 34–58 (2015), 10.1111/nph.13003.
- I. S. Jónsdóttir, O. Khitun, A. Stenstrom, Biomass and nutrient responses of a clonal tundra sedge to climate warming. *Botany* **83**, 1608–1621 (2005), 10.1139/b05-129.
- M. C. McCarthy, B. J. Enquist, Consistency between an allometric approach and optimal partitioning theory in global patterns of plant biomass allocation. *Funct. Ecol.* **21**, 713–720 (2007), 10.1111/j.1365-2435.2007.01276.x.
- S. Hong *et al.*, Divergent responses of soil organic carbon to afforestation. *Nat. Sustain.* **3**, 694–700 (2020), 10.1038/s41893-020-0557-y.

41. R. D. Hollister, K. J. Flaherty, Above- and below-ground plant biomass response to experimental warming in northern Alaska. *Appl. Veg. Sci.* **13**, 378–387 (2010), 10.1111/j.1654-109X.2010.01079.x.
42. H. Liu *et al.*, Simulating warmer and drier climate increases root production but decreases root decomposition in an alpine grassland on the Tibetan plateau. *Plant Soil* **458**, 59–73 (2021), 10.1007/s11104-020-04551-y.
43. J. R. Deslippe, M. Hartmann, W. W. Mohn, S. W. Simard, Long-term experimental manipulation of climate alters the ectomycorrhizal community of *Betula nana* in Arctic tundra. *Global Change Biol.* **17**, 1625–1636 (2011), 10.1111/j.1365-2486.2010.02318.x.
44. H. Yun *et al.*, Warming, permafrost thaw and increased nitrogen availability as drivers for plant composition and growth across the Tibetan Plateau. *Soil Biol. Biochem.* **182**, 109041 (2023), 10.1016/j.soilbio.2023.109041.
45. H. Muraoka *et al.*, Photosynthetic characteristics and biomass distribution of the dominant vascular plant species in a high Arctic tundra ecosystem, Ny-(A)over-circlealesund, Svalbard: Implications for their role in ecosystem carbon gain. *J. Plant Res.* **121**, 137–145 (2008), 10.1007/s10265-007-0134-8.
46. M. H. Chandregowda *et al.*, Belowground carbon allocation, root trait plasticity, and productivity during drought and warming in a pasture grass. *J. Exp. Bot.* **74**, 2127–2145 (2023), 10.1093/jxb/erad021.
47. R. M. Marchin *et al.*, Extreme heat increases stomatal conductance and drought-induced mortality risk in vulnerable plant species. *Global Change Biol.* **28**, 1133–1146 (2022), 10.1111/gcb.15976.
48. F. L. Marchand, S. Mertens, F. Kockelbergh, L. Beyens, I. Nijs, Performance of High Arctic tundra plants improved during but deteriorated after exposure to a simulated extreme temperature event. *Global Change Biol.* **11**, 2078–2089 (2005), 10.1111/j.1365-2486.2005.01046.x.
49. L. C. Hicks, M. Yuan, A. Brangari, K. Rousk, J. Rousk, Increased above- and belowground plant input can both trigger microbial nitrogen mining in subarctic tundra soils. *Ecosystems* **25**, 105–121 (2022), 10.1007/s10021-021-00642-8.
50. N. Tim, P. Oppenheimer, A. Etard, J. J. Williams, Tropical and Mediterranean biodiversity is disproportionately sensitive to land-use and climate change. *Nat. Ecol. Evol.* **4**, 1630–1638 (2020), 10.6084/m9.figshare.12674372.
51. J. M. Chase, S. A. Blowes, T. M. Knight, K. Gerstner, F. May, Ecosystem decay exacerbates biodiversity loss with habitat loss. *Nature* **584**, 238–243 (2020), 10.1038/s41586-020-2531-2.
52. L. Ding, J. Zhou, X. Zhang, S. Liu, R. Cao, A long-term 0.01° surface air temperature dataset of Tibetan Plateau. *Data Brief* **20**, 748–752 (2018), 10.1016/j.dib.2018.08.107.
53. Y. Du, J. Yi, *Data of Climatic Factors of Annual Average Temperature in the Xizang (1990–2015)* (National Tibetan Plateau Data Center, Beijing, China, 2019).
54. Q. Wu, T. Zhang, Changes in active layer thickness over the Qinghai-Tibetan Plateau from 1995 to 2007. *J. Geophys. Res.-Atmos.* **115**, D09107 (2010), 10.1029/2009JD012974.
55. H. Duan *et al.*, Spatial and temporal differences in alpine meadow, alpine steppe and all vegetation of the Qinghai-Tibetan Plateau and their responses to climate change. *Remote Sens.* **13**, 669 (2021), 10.3390/rs13040669.
56. M. Shen *et al.*, Plant phenology changes and drivers on the Qinghai-Tibetan Plateau. *Nat. Rev. Earth Environ.* **3**, 633–651 (2022), 10.1038/s43017-022-00317-5.
57. M. Shen, S. Piao, N. Cong, G. Zhang, I. A. Jassens, Precipitation impacts on vegetation spring phenology on the Tibetan Plateau. *Global Change Biol.* **21**, 3647–3656 (2015), 10.1111/gcb.12961.
58. T. Essington *et al.*, Historical reconstruction of the Puget Sound (USA) groundfish community. *Mar. Ecol. Prog. Ser.* **657**, 173–189 (2021), 10.3354/meps13547.
59. C. M. O'Reilly *et al.*, Rapid and highly variable warming of lake surface waters around the globe. *Geophys. Res. Lett.* **42**, 10773–10781 (2015), 10.1002/2015GL066235.
60. S. N. Wood, *Generalized Additive Models: An Introduction with R* (CRC Press, 2017).
61. E. J. Pedersen, D. L. Miller, G. L. Simpson, N. Ross, Hierarchical generalized additive models in ecology: An introduction with mgcv. *PeerJ* **7**, e6876 (2019), 10.1029/2009JD012974.
62. L. Liu *et al.*, Permafrost degradation diminishes terrestrial ecosystem carbon sequestration capacity on the Qinghai-Tibetan plateau. *Global Biogeochem. Cycles* **36**, e2021GB007068 (2022), 10.1029/2021GB007068.
63. B. D. Martín *et al.*, LPJ-GUESS/LSMv1.0: A next-generation land surface model with high ecological realism. *Geosci. Model Dev.* **15**, 6709–6745 (2022), 10.5194/gmd-15-6709-2022.
64. M. Guimberteau *et al.*, ORCHIDEE-MICT (v8. 4.1), a land surface model for the high latitudes: Model description and validation. *Geosci. Model Dev.* **11**, 121–163 (2018), 10.5194/gmd-11-121-2018.
65. G. Krinner *et al.*, A dynamic global vegetation model for studies of the coupled atmosphere-biosphere system. *Global Biogeochem. Cycles* **19**, GB1015 (2005), 10.1029/2003GB002199.
66. H. Yun, W. Qingbai, B. Elberling, C. M. Zohner, Changes in above- versus belowground biomass distribution in permafrost regions in response to climate warming [Dataset]. Zenodo. <https://doi.org/10.5281/zenodo.11218337>. Accessed 20 May 2024.